Journal of Membrane Science 668 (2023) 121214

Contents lists available at ScienceDirect

Journal of Membrane Science

journal homepage: www.elsevier.com/locate/memsci

Tuning charge density in tethered electrolyte active-layer membranes for enhanced ion-ion selectivity

Cassandra J. Porter [a,b,*], Li Wang [a], Mingjiang Zhong [a,c], Menachem Elimelech [a]

[a] Department of Chemical and Environmental Engineering, Yale University, New Haven, CT, 06520-8286, United States
[b] Department of Chemical Engineering, Auburn University, Auburn, AL, 36849-5341, United States
[c] Department of Chemistry, Yale University, New Haven, CT, 06520-8286, United States

ARTICLE INFO

Keywords:
Tethered-electrolyte active-layer membranes
Surface-initiated atom transfer radical polymerization
Polyelectrolyte
Selectivity
Polymer brush

ABSTRACT

Efforts toward developing membranes for aqueous separations beyond desalination have intensified, in attempts to achieve zero liquid discharge and a circular economy. Treatment of unconventional wastewaters and brines as well as recovery of valuable species require separation of solutes and ions. Recently, tethered electrolyte active-layer membranes (TEAMs) with dense ionizable brush polymers grafted from cellulose ultrafiltration supports were introduced as a robust, highly controllable membrane platform for these aqueous separations. In this study, we investigate crosslinking of single-block TEAMs to increase the effective charge density and coverage of pores by the active layer, and to possibly tap into size-based exclusion mechanisms. We also determine if crosslinking multiblock TEAMs comprising block copolymers of both negative and positive charge can better align blocks, thereby improving ion rejection. Single-block TEAMs with relatively short crosslinkers proved to have the highest divalent co-ion rejection in dilute solutions, at ~85–95%. NaCl was rejected ~55 and 80% by crosslinked negatively- and positively-charged TEAMs, respectively. Anion monovalent selectivity, Cl^-/SO_4^{2-}, was as high as ~25 for negative TEAMs, while the maximum Na^+/Ca^{2+} ratio achieved by positive TEAMs was ~9.5. This work reinforces the value of ultrathin brush active-layer membranes and TEAMs as important tools to understand fundamental transport through membranes and better control synthesis for targeted selectivity.

1. Introduction

Current commercial thin-film composite reverse osmosis (TFC-RO) membranes require only about double the minimum energy of separating salt from seawater [1], permeating water 10^4–10^5 times faster than macromolecules and ions [2–4]. No other membrane materials have come close to competing with the capability of aromatic polyamide to desalinate sea and brackish water, and the energy efficiency and cost of desalination may only incrementally improve with further development of membrane materials [5]. However, other aqueous separations are of interest in achieving a circular economy and zero liquid discharge [6]. The ability to remove specific valuable ions or toxic chemicals from complex waste streams and untraditional water sources is imperative for these environmental conservation efforts [4,6]. Species of value include nitrate- and phosphate-rich nutrients from municipal wastewater streams, which are important as fertilizers used in food production [7]. Lithium found in produced water from oil and gas extraction as well as copper and rare earth elements like yttrium found in acid mine drainage are also of growing importance [8–10]. These elements are crucial for the production of electronics, electric vehicles, and clean energy components like permanent magnets in wind turbines, which are vital technologies to combat global warming and pursue environmental sustainability [10].

In each of these separations, selective retention of a specific solute is required. While TFC-RO membranes can reject salt nearly completely, they cannot selectively distinguish between ions. Additionally, TFC-RO membranes cannot sufficiently reject certain species in waters to meet regulatory limits for potable use and irrigation, such as boron [4,11]. Furthermore, because aromatic polyamide has a limited density of reactive functional groups (i.e., carboxyls and unreacted amines) [12,13], tuning interfacially-polymerized TFC-RO membranes after their formation is complicated. Nanofiltration (NF) and ion-exchange membranes are of interest for solute-solute separations but require some further tailoring for the niche applications mentioned above [14–17]. Additionally, polyelectrolyte multilayer membranes (PEMs) and self-assembled membranes of random zwitterionic amphiphilic

* Corresponding author. Department of Chemical Engineering, Auburn University, Auburn, AL, 36849-5341, United States.
E-mail address: cjp0084@auburn.edu (C.J. Porter).

https://doi.org/10.1016/j.memsci.2022.121214
Received 20 September 2022; Received in revised form 17 November 2022; Accepted 21 November 2022
Available online 24 November 2022

copolymers (*r*-ZACs) have proven instrumental in developing unique active layers with varied functionalities and charge [18–25].

PEMs comprise layers of alternately-charged polymers that are built up layer-by-layer through electrostatic attraction and entropic gains [26–31]. PEMs can be prone to swelling and disintegration under extreme pH and high salinity conditions [32,33], such that performance is compromised unless strategies to stabilize these layers are used. Meanwhile, random/statistical copolymers of zwitterionic and hydrophobic repeat units in *r*-ZAC-based membranes drive the self-assembly of bicontinuous hydrophobic and hydrophilic nanodomains [34–38]. Zwitterionic microphases provide water pathways while rejecting neutral solutes >1 kDa, equating to a pore size of ~1.5 nm [36,37,39,40].

Attempts to achieve smaller pore sizes for ion rejection by adjusting *r*-ZAC copolymer proportion/composition have proven fruitless [36,37], necessitating further modification after self-assembly [38]. Crosslinking has helped stabilize PEMs and improve ion rejection and selectivity [41–44], while increasing bilayer quantity can enhance rejection to within RO range for dilute saline solutions [45,46]. Self-assembled zwitterionic membranes with cross-linkable hydrophobic functionalities have also achieved impressive rejection of divalent co-ions and unprecedented monovalent/divalent selectivity for a scalable polymeric system, with >99.2% SO_4^{2-} rejection and a Cl^-/SO_4^{2-} selectivity of 101 [38]. However, these optimization tactics for PEMs and *r*-ZAC-based membranes have caused permeability below that of TFC-RO, exhibiting the selectivity-permeability tradeoff common to polymeric membranes [47,48]. The requirement of opposite charges within PEMs and *r*-ZAC-based membranes also complicates fundamental understanding of transport and somewhat limits tailor-ability.

Recently, we introduced tethered electrolyte active-layer membranes (TEAMs) as an alternative polyelectrolyte membrane [49]. TEAMs are composed of densely grafted ionizable brush polymers covalently tethered to a porous support that act as the selective barrier. We used surface-initiated atom transfer radical polymerization (SI-ATRP) to graft-from a cellulosic ultrafiltration substrate. Cellulose was a fitting surface with a dense distribution of hydroxyl groups, used elsewhere for production of brush polymers to alleviate membrane fouling, alter pore sizes in the ultrafiltration range, and increase adsorption of targeted proteins [50–53]. SI-ATRP has also been used to produce antifouling poly(sulfobetaine methacrylate) zwitterion brushes on polyacrylonitrile ultrafiltration supports, with passive ion diffusion suggesting selectivity that followed the Hoffmeister series for anions, although this was not confirmed under hydraulic pressure [54].

The strengths of SI-ATRP arise from its mechanism. SI-ATRP is a type of living radical polymerization where a surface-tethered initiator has a cleavable end-group (usually a halogen) that is removed by a metal/ligand complex to form a chain-end radical. This activated end reacts with a monomer, propagating the radical before the metal/ligand/halogen complex reattaches the halogen to the chain end [55–57]. The back-and-forth between activated and deactivated states, with deactivation faster than activation, causes a small ratio of radical-to-dormant chains at any one time, at a concentration of only 10^{-4}–10^{-6} [57,58]. This results in low rates of termination and produces polymers of relatively low dispersity (*Đ*), often <1.2. Low *Đ* and the fact the initiation point propagates down the chain make ATRP ideal for production of distinct block copolymers [59–65].

We initially hypothesized that well-aligned multiblocks of alternating charge within TEAMs would reject salt more than PEMs and require fewer blocks for optimization than the equivalent number of bilayers used in PEMs. However, we showed that single-block TEAMs of positive poly((2-(methacryloyloxy)ethyl)trimethylammonium iodide) (PMOTA) and negative poly(methacrylic acid) (PMAA) rejected salt with no membrane swelling [49]. Unlike PEMs and *r*-ZAC-based membranes, TEAMs uniquely do not require oppositely charged functional groups for self-assembly, and position like-charges close enough together to induce co-ion rejection. In fact, we observed diminishing salt retention with increasing block number, which was primarily attributed to the collapse of brushes such that oppositely charged functionalities would be closest to each other and cause charge-screening in a more entropically favorable state.

To combat the collapse of brush polymers in multiblock TEAMs, we next hypothesized that crosslinking could be used to force block alignment and maximize salt rejection. Crosslinking of both multi- and single-block TEAMs might also better place polymers over pore mouths, where coverage by the active layer is most critical. Better pore coverage means that ions encounter an effectively higher density of charged groups, which is crucial in maximizing salt rejections that are primarily dictated by the Donnan effect. Lastly, crosslinking may also tap into size-based exclusion mechanisms for both multi-and single-block TEAMs. Single-block TEAMs without crosslinking have had molecular weight cutoffs (MWCOs) of a minimum of 3 kDa [49], equating to a pore size of ~3 nm. Meanwhile, NF membranes that show higher salt rejection have pores of 0.5–1 nm diameter, typically rejecting polysaccharides in the range of hundreds of Daltons [66,67].

In this study, we further investigate how to optimize ion rejection and monovalent selectivity of TEAMs by developing two different crosslinking approaches that are specific to the two polymers considered, producing single-block TEAMs of positive, crosslinked poly((2-(methacryloyloxy)ethyl)trimethylammonium iodide) (*x*PMOTA) or negative poly(methacrylic acid) with a random distribution of crosslinked poly(2-hydroxyethyl methacrylate) (PMAA-*co*-*x*PHEMA). Additionally, we produced a diblock TEAM comprising a negative base block and terminating, crosslinked positive block (PMAA-*b*-*x*PMOTA). We varied both the proportion and length of the crosslinkers used during synthesis. After verifying the production of these polymers by compositional analysis of homogeneous analogues (i.e., bulk-solution polymers) and membrane surface characterization, we tested membrane performance. Water permeability, salt rejection, molecular weight cutoff, and monovalent ion selectivity were evaluated. This work further optimizes a relatively new form of polyelectrolyte membrane with the potential to enhance understanding of fundamental membrane transport and provide a platform for high tailor-ability toward ion-ion selectivity. Single-block TEAMs with one type of charge may prove instrumental in separating valuable heavy metals and rare earth elements through coordination chemistry, demonstrated previously with PEMs [31]. Multiblock TEAMs could also serve as scaffolds for the integration and alignment of nanomaterials, especially bioinspired nanochannels in defect-free biomimetic membranes synthesized from bottom-up [68].

2. Materials and methods

2.1. Chemicals and materials

Adipoyl chloride (AC), malonyl chloride (MC), 1,6-diiodohexane, 1,2-diiodoethane, methyl iodide, α-bromoisobutyryl bromide (BiBB), triethylamine (TEA), *N*,*N*,*N*′,*N*″,*N*″-pentamethyldiethylenetriamine (PMDETA), copper(I) and copper(II) bromides (Cu(I) and Cu(II)), ethyl α-bromoisobutyrate (EBiB), 2-(dimethylamino)ethyl methacrylate (DMAEMA), *tert*-butyl methacrylate (*t*BMA), trifluoroacetic acid, diethyl ether, glacial acetic acid, poly(ethylene glycol) (PEG) of varied molecular weights (MW), and calcium chloride ($CaCl_2$), were purchased from Sigma-Aldrich (St. Louis, MO, USA). L(+)-ascorbic acid and HPLC-grade tetrahydrofuran (THF) were acquired from Fisher Scientific (Fair Lawn, NJ, USA). Dimethyl formamide (DMF) and polytetrafluoroethylene (PTFE) syringe filters (0.45 μm MWCO) were purchased from VWR International (Radnor, PA, USA). Deuterated chloroform ($CDCl_3$, 99.8%) and dimethyl sulfoxide (DMSO-d_6, 99.9%) were provided by Cambridge Isotope Laboratories (Andover, MA, USA). Basic and neutral alumina were purchased from Sorbtech (Norcross, GA, USA). Composite regenerated cellulose ultrafiltration membranes (Ultracel) of 10 kDa MWCO were produced by EMD Millipore (Darmstadt, Germany). Acetone and dichloromethane (DCM) were purchased from Macron Fine Chemicals

while 2-propanol, sodium chloride (NaCl), and sodium sulfate (Na_2SO_4) came from J.T. Baker, divisions of Avantor Performance Materials (Center Valley, PA, USA). Nitrogen was provided by Airgas East (Salem, NH, USA). Deionized (DI) ultra-filtered water (>18.2 MΩ cm) was prepared through passage in a Milli-Q system with Elix Technology (Integral 10, EMD Millipore, Billerica, MA, USA) and utilized throughout synthesis and experimentation.

Chemicals were used as purchased, except monomers, Cu(I), and membranes. Before conducting polymerization reactions, monomers were passed through a basic alumina column to remove inhibitor. Cu(I) was prepared by stirring a suspension of 1 equiv Cu(I) with 2 equiv L (+)-ascorbic acid in DI water for 15 min and filtering out the white product. The product was consecutively washed with DI water, glacial acetic acid, and diethyl ether. After vacuum drying the Cu(I), it was stored in darkness under nitrogen until use. Cellulose membranes were cut into squares of ~25 cm^2 and thoroughly rinsed overnight in 1:1 (v/v) 2-propanol:DI water on a shake plate before initiator bonding and polymerization.

2.2. Synthesis of crosslinked tethered electrolyte active-layer membranes

Previously developed synthesis methods were slightly modified to produce the single-block TEAMs in this study [49,69]. In our first proof-of-concept study on TEAMs, we investigated growth on cellulosic membranes of varied MWCO and showed that initial support pore size had little effect on resultant salt rejection and pure water permeability [49]. However, in the present study, where full coverage of pores with crosslinked brush polymers was key to optimizing salt rejection and selectivity, we selected the smallest MWCO available for cellulose supports of 10 kDa. First, initiator and crosslinker were competitively bonded to provide surface initiation points for ATRP and stabilize the membrane within organic solvents, as previously described [49,69]. In brief, in an oxygen-free, nitrogen-rich environment, membranes were reacted with crosslinker AC and initiator BiBB in THF with excess of scavenger ligand TEA for 12 h overnight on a shake plate in an oven set at 40 °C. A ratio of 55% of acyl halides attributed to BiBB and 45% attributed to AC was used (Fig. 1a) [69]. The reaction on the cellulosic supports was quenched in fresh THF and consecutively washed for 0.5 h each in acetone, isopropanol, and water on a shake plate.

Based on our previous study [49], PDMAEMA and P*t*BMA were once again used as precursors for positively- and negatively-charged blocks, respectively, polymerized using the same SI-ATRP methods (Fig. 1b and c). Simultaneously-conducted homogeneous ATRP reactions with initiator EBiB (for P*t*BMA) or a macroinitiator comprising a known molecular weight of P*t*BMA (for PDMAEMA) were used as a proxy to determine the molecular weights of each polymer. Proportions of monomer, solvent DMF, initiator EBiB or macroinitiator P*t*BMA, ligand PMDETA, and activating and deactivating metals Cu(I) and Cu(II) were adjusted to achieve a targeted degree of polymerization (DP) of ~1000 and maintain low $Đ$. This targeted DP is ~1.5 times larger than we previously targeted to ensure crosslinked brush polymers could fully reach across support pores. For PDMAEMA, two reactions in a row were necessary at 40 °C for 24 h under constant nitrogen bubbling since synthesis halted at <50% conversion for each reaction, just as previously reported [49]. Reagent proportions used to reach the targeted DP were 1 μmol of macroinitiator, 80 mL of monomer DMAEMA, 70 mL of DMF, 9 mL of co-solvent water (shown to improve conversion), 70 mg of Cu(I), 20 mg of Cu(II), and 0.14 mL PMDETA.

To produce *x*PMOTA, the membranes were rinsed for 5 min in 12% trifluoroacetic acid (TFA) in DCM to remove copper, an inhibitor of quaternization [49]. After rinsing in fresh DCM and DMF, the brush polymers were quaternized with various ratios of di-functionalized crosslinkers of either 1,6-diiodohexane (longer crosslinker) or 1,2-diiodoethane (shorter crosslinker) and methyl iodide. To describe methyl iodide versus crosslinker proportions used, we have defined a molar percentage of halogens attributed to methyl iodide as $\%MI_{Halogen}$, or halogens that purely quaternize without crosslinking, compared to the ratio of sidechains utilized for crosslinking:

$$\%MI_{Halogen} = \frac{[MI]}{[MI] + 2[x\text{linker}]} \times 100 \quad [1]$$

where concentrations are molar. This strategy using competitive bonding maintained the same number of steps for synthesis of both crosslinked and un-crosslinked PMOTA TEAMs and allowed for crosslinker density to be controlled by proportionality rather than reaction duration. Quaternization solutions contained a total of crosslinker plus methyl iodide of ~0.5 vol% in DMF, with $\%MI_{Halogen}$ in the range of 80–100 mol%. Membranes were immersed in these solutions for 24 h on a shake plate before thoroughly rinsing in fresh DMF, acetone, isopropanol, and finally water.

For P*t*BMA, the *tert*-butyl ester side groups are less reactive and thus could require multiple steps for crosslinking and converting into charged carboxyl groups. If these groups are cleaved into carboxyl groups and then only partially crosslinked through esterification reactions, the reliance on time as the variable to control crosslinker density could render the process insufficiently reproducible as well as induce an asymmetric distribution of crosslinkers based on diffusion rates. Furthermore, quantifying resultant crosslinker density in a system with such a nonideal support could prove challenging, so choosing methods whereby proportionality had the greatest chance of controlling relative crosslinker density was important. Thus, various proportions of HEMA monomer were copolymerized to produced hydroxyl sidechains for later crosslinking (Fig. 1c). The reagent proportions used were 40 mL *t*BMA, 80 mL DMF, 70 mg Cu(I), 20 mg Cu(II), 0.14 mL PMDETA, 13 μL EBiB, and various molar proportions of HEMA in the range of 0–28 mol %. The reaction was carried out at 50 °C for 45 min in an oxygen-free environment with constant nitrogen bubbling. Analogous to Eq. (1), we defined the %*t*BMA compared to HEMA used during the synthesis as a relative metric for describing carboxyl groups per chain versus sidechains used in crosslinking:

$$\%t\text{BMA} = \frac{[t\text{BMA}]}{[t\text{BMA}] + [\text{HEMA}]} \times 100 \quad [2]$$

where concentrations are molar.

After production of P*t*BMA copolymerized with PHEMA (P*t*BMA-*co*-PHEMA), PHEMA was then crosslinked in THF using either adipoyl chloride (longer crosslinker) or malonyl chloride (shorter crosslinker). This crosslinking reaction used the same procedure as during the initiator and crosslinker bonding on cellulose, with scavenger TEA but excluding BiBB [69]. To convert P*t*BMA into negatively charged PMAA, *tert*-butyl ester bonds were selectively cleaved in 12 vol% TFA in DCM for 24 h, which is a common deprotection reaction involving *tert*-butyloxycarbonyls [69,70]. The resulting polymer is considered PMAA copolymerized with crosslinked PHEMA, or PMAA-*co*-*x*PHEMA.

2.3. Characterization of membranes and polymers

Since homogeneous polymer analogues have been shown to be similar in molecular weight and $Đ$ to heterogeneous brushes produced within the same reaction environment [71–75], bulk homogeneous P*t*BMA analogues were directly characterized by gel permeation chromatography (GPC, EcoSEC HLC-8320GPC, Tosoh Bioscience, Tokyo, Japan). Polymer samples were passed through neutral alumina and filtered before running through the GPC column to determine the relative number average molecular weight (M_n), weight average molecular weight (M_w), and $Đ$. Polystyrene (PS) standards were used for calibration with a PS immobile phase and THF. Although PHEMA does show stronger interaction than P*t*BMA with the PS immobile phase, and consequently pure PHEMA polymers sometimes cannot be identified in organic-phase GPC, the percentage of copolymerized PHEMA used did not prevent measurement via GPC. However, PDMAEMA does strongly

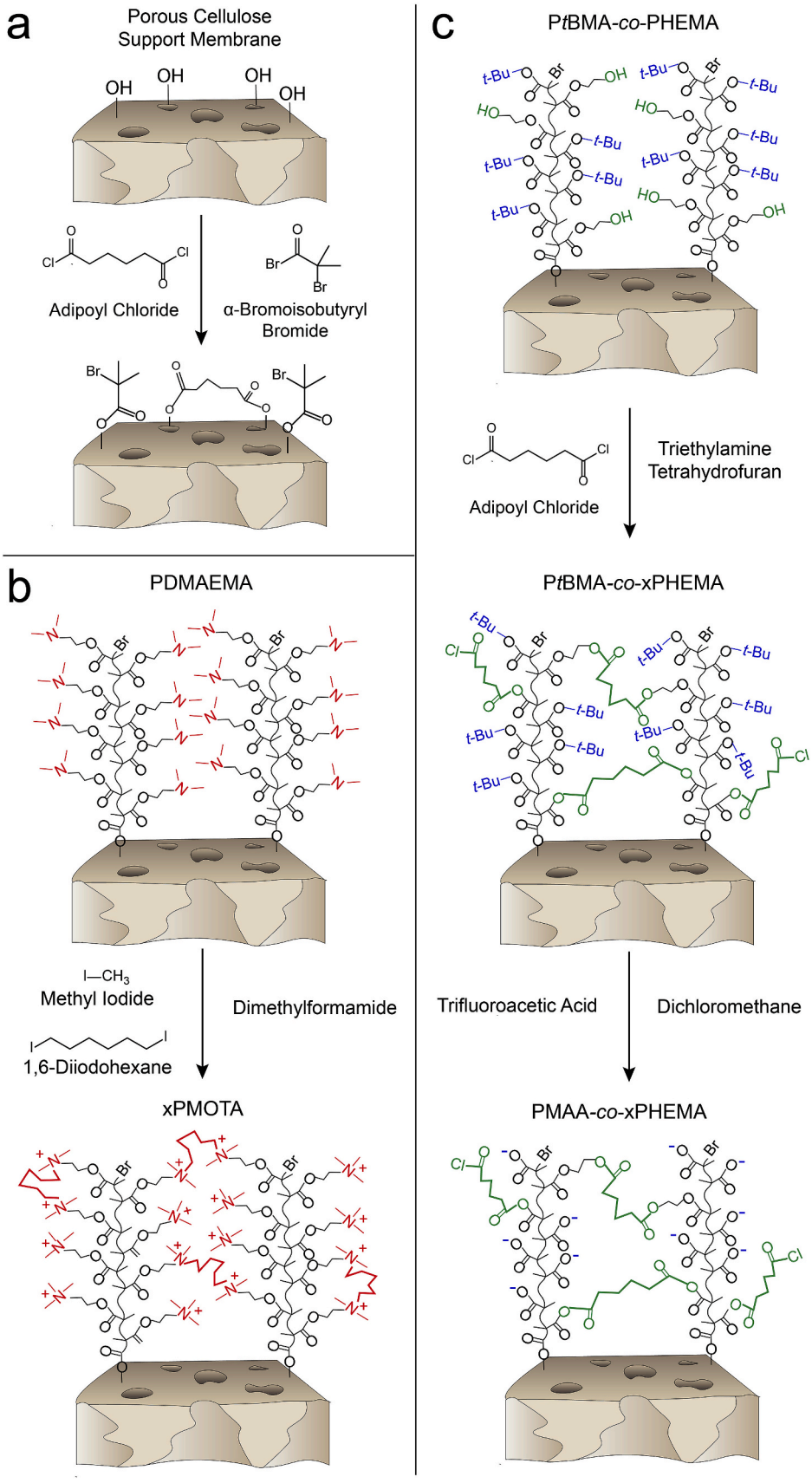

Fig. 1. Synthesis scheme for single-block tethered electrolyte active-layer membranes (TEAMs) with crosslinking. (a) Preparation of cellulose support through esterification of adipoyl chloride crosslinker for stabilization and α-bromoisobutyryl bromide as a polymerization initiator. (b) Production of a positively-charged, crosslinked TEAM of poly(2-(methacryloyloxy)ethyl triethylammonium iodide) (*x*PMOTA). A neutral precursor of poly(2-dimethylaminoethyl methacrylate) (PDMAEMA) is first grown through surface-initiated atom-transfer radical polymerization (SI-ATRP) and then quaternized with a specific proportion of difunctionalized crosslinker and methyl iodide. 1,6-diiodohexane is shown as crosslinker here, but 1,2-diiodoethane was also considered in this study. Grafting-from of precursor polymers for crosslinked TEAMs from porous cellulosic supports. (c) Production of a negatively-charged, crosslinked TEAM. A neutral precursor poly(*tert*-butyl methacrylate) (P*t*BMA) was copolymerized with a specific proportion of poly(2-hydroxyethyl methacrylate) (PHEMA). Hydroxyl groups were crosslinked through an esterification reaction with either adipoyl chloride (shown here) or a shorter crosslinker of malonyl chloride. *Tert*-butyl ester groups were then selectively cleaved in trifluoroacetic acid to produce carboxyl groups in the final product of poly(methacrylic acid) copolymerized with crosslinked PHEMA (PMAA-*co*-*x*PHEMA).

interact with PS, such that GPC could not be used to analyze homogeneous analogues of the PMOTA precursors.

Instead, to determine the relative molecular weight of PDMAEMA, ^{1}H NMR spectroscopy was used, as previously demonstrated elsewhere [49] (See *Supplementary Data*, Figs. S1–2). Imperative for this method was the use of a macroinitiator of P*t*BMA of known molecular weight in order to compare the relative proton signals that were specific to P*t*BMA with those of the added PDMAEMA blocks. This macroinitiator was prepared by ATRP, passed through neutral alumina to remove copper, and precipitated in methanol. It was then partially dried, redissolved in a known proportion of DMF, and used in subsequent reactions with DMAEMA in bulk. Only single blocks of PDMAEMA were grown from the cellulosic surfaces. After addition of the PDMAEMA block in the same environment as the SI-ATRP of PDMAEMA on cellulose, the bulk block copolymer product was passed through neutral alumina, precipitated in 1:1 (v/v) methanol:water, rinsed, and redissolved in DMF, followed by repeating precipitation and rinsing. The product was dried for 24 h under vacuum before taking ^{1}H NMR measurements (Agilent DD2 400 MHz NMR Spectrometer) using $CDCl_3$.

Changes in water contact angles and pure water permeability for modified membranes were used as qualitative indicators of successful brush polymer synthesis, conversion into charged polymers, and controlled proportion of crosslinking. Water contact angles were recorded using a sessile drop method (1 μL drops) with a contact angle goniometer (Theta with OneAttension software, Biolin). Membrane samples were first dried through solvent exchange from water to acetone by soaking for 30 min in 1:1 (v/v) water:isopropanol, 1:1 (v/v) isopropanol:acetone, then finally pure acetone before drying under vacuum for 24 h. Dried samples were secured to microscope slides with double-sided tape. Droplets were imaged every 0.3 s for a total of 10 s, and left- and right-side water contact angles were measured for each image and averaged. On 5−7 separate locations for each membrane type, droplets were measured in this way and averaged.

The addition of brush polymers was expected to obstruct support pores and reduce effective pore size, decreasing permeate flux. To verify expectation, samples were punched into circles of 4.5 cm diameter (effective testing area of 13.4 cm^2), and a dead-end filtration cell (Amicon® Stirred Cell, 50 mL, ~5 bar maximum pressure) was used to measure pure water permeability at 1.4 bar for bare commercial cellulose membranes and 2 bar for modified membranes. Only 10 min of permeation were necessary to reach steady state, as insignificant compaction of membranes was observed.

To detect the presence of characteristic functional groups and investigate whether changes in crosslinking density could be qualitatively detected, attenuated total reflection Fourier-transform infrared spectroscopy (ATR-FTIR, Shimadzu IRTracer-100, diamond crystal) was conducted on dry, modified membranes. For these measurements, samples were dried using the same procedure as used when preparing for water contact angle measurements. ATR-FTIR background measurements were taken as bare cellulose membrane. Absorbance rather than transmittance was used, at a resolution of 1 cm^{-1} with a total of 20 measurements taken per sample. Two locations on each sample were tested to ensure signals were consistent.

2.4. Ion rejection and selectivity performance assessment

Salt rejections of modified membranes were also conducted using the same dead-end cell, with a stir rate of 350 rpm and hydraulic pressure of 2 bar. NaCl, $CaCl_2$, and Na_2SO_4 were individually tested at a concentration of 2 mM. Feed and permeate conductivities were determined using a conductivity probe and correlated to salt concentration. Since the concentration in the feed side of the dead-end vessel increased during testing, only 1 mL of permeate was passed to reach steady-state transport and minimize change in feed concentration before collecting permeate samples of ~3–4 mL. To better reflect actual observed rejection, initial and final feed concentrations were averaged as an effective feed concentration. Ion chromatography (IC) for cations (Dionex ICS-1000) and anions (Metrohm 930 Compact IC Flex) was regularly used on random permeate and feed samples to verify that conductivity measurements correlated to concentrations within ±3% of accurate values. Observed rejection R_o was calculated as

$$R_o = 1 - \frac{C_P}{C_F} \quad [3]$$

where C_P is the permeate concentration and C_F is the effective feed concentration from averaged initial feed and final retentate values.

Two strategies were used to suggest the degree to which Donnan versus size-based exclusion mechanisms contributed to salt rejection. First, the MWCO of bare and modified membranes was estimated using the dead-end cell with operating conditions described above by determining the rejection of neutral solutes with varied MWs. These neutral solutes comprised raffinose of 0.5 kDa and larger, varied sizes of poly (ethylene glycol) (PEG), all at a feed concentration of 1000 ppm. A total organic carbon analyzer (Shimadzu TOC–VCSH Analyzer) was used to determine retentate, feed, and permeate concentrations of neutral solutes from calibration curves for each pertinent solute. Eq. (3) was then used to calculate observed rejection. MWCO was interpolated as the molecular weight of PEG rejected at 90%.

Changes in salt rejection with varied Debye length were also probed as an indication of Donnan exclusion. Since the Debye length decreases logarithmically with increase in concentration, concentration was varied by orders of magnitude from 0.2 to 20 mM. The Debye length λ_D was calculated using the Debye–Hückel equation:

$$\lambda_D = \kappa_D^{-1} = \left(\frac{\varepsilon_0 \varepsilon_r k_B T}{e^2 \sum_i n_{0,i} z_i^2} \right)^{1/2} \quad [4]$$

where κ_D is the inverse of the Debye screening length, ε_0 is the permittivity of free space, ε_r is the relative permittivity, or dielectric constant, of the solvent (for water at 25 °C, $\varepsilon_r = 78.5$), k_B is the Boltzmann constant, T is the solvent temperature, e is the elementary charge constant, $n_{0,i}$ is the bulk number density of ionic species i found by multiplying Avogadro's number by the species concentration in mol/m^3 ($n_{0,i} = N_A c_i$), and z_i is the charge number of ion species i. A hydraulic pressure of 2 bar and a stir rate of 350 rpm was used for these experiments, while R_o was calculated with Eq. (3).

Ion selectivity of monovalent versus divalent co-ions was calculated from single-salt solutions (ideal selectivity) and from salt mixtures (mixed selectivity). For mixtures, co-ions were maintained at a total of 2 mM while adjusting molar proportions of divalent versus monovalent co-ions to 25, 50, and 75%. Selectivity S was calculated using [32].

$$S_{i/j} = \frac{C_{F,j}}{C_{P,j}} \Big/ \frac{C_{F,i}}{C_{P,i}} = \frac{1 - R_{o,i}}{1 - R_{o,j}} \quad [5]$$

where i represents the monovalent co-ion and j represents the divalent co-ion. For mixtures of salts, concentrations in the feed and permeate were measured using IC rather than conductivity to distinguish ions.

To describe the salt rejection as a function of feed salt concentration, we also employed the Donnan-steric-pore model (DSPM) that considers both Donnan effects and steric exclusion [76,77]. The transport phenomena were modeled based on the extended Nernst-Planck equation. In this study, we only considered the brush layer as the active layer since the substrate cellulosic membrane barely rejects salt. Development of the DSPM and determination of active-layer properties including pore size, charge density, porosity, and effective membrane thickness are detailed in the *Supplementary Data*.

3. Results and discussion

3.1. Analysis of brush layers

In our first proof-of-concept study of TEAMs, we established the methods by which single blocks of brush polymers composed of P*t*BMA and PDMAEMA were prepared and modified into charged PMAA and PMOTA, respectively [49]. SI-ATRP conditions were previously optimized to maintain membrane stability and achieve maximized salt rejection with the minimal DP necessary. In the present study, we modified SI-ATRP reagent proportions to achieve brush polymers of a slightly greater DP. Using GPC to measure M_n of homogeneous P*t*BMA analogues, the ATRP reactions used to produce multiple batches of P*t*BMA-*co*-PHEMA resulted in DP = 1300 ± 60 and $Đ$ = 1.31 ± 0.07. Diblock copolymers of P*t*BMA-*co*-PDMAEMA were produced simultaneously in the same environments as our SI-ATRP-produced brush polymers of PDMAEMA so that comparison of characteristic proton peaks using ^{1}H NMR spectroscopy could reveal the approximate molecular weight of PDMAEMA. The reaction procedures used resulted in ~50% of the total diblock being attributed to PDMAEMA, so we assume that DP is also approximately 1300 (although standard deviation and $Đ$ were not deduced).

In previous work, active-layer thickness was conservatively estimated as double the radius of gyration for polymer in good solvent [1]. Assuming a statistical segment length, or Kuhn monomer length, identical to that reported for poly(methyl methacrylate) of 0.65 nm with a Gaussian coil conformation [78,79], double the radius of gyration would be ~19 nm at this DP. However, we know that brush layers take on different conformations depending on grafting density, whereby neighboring chains interact with each other, causing polymer elongation. This is especially true for like-charged polyelectrolyte brushes that mutually repulse each other, such that at a high grafting density, polymer chain elongation causes brush height to approach the maximal polymer contour length [80]. We therefore estimate a brush height of ~290 nm (see *Supplementary Data* for details). This estimation, which assumes polymer orientation normal to the cellulosic surface, does not account for the possible abnormal orientation of polymers around pore rims. There are also likely conformational effects due to asymmetric distribution of charged functional groups, as seen for densely crowded, ionizable brush polymers [81], such that greater elongation may occur closer to bulk saline solutions and diminish within the depth of the polymer.

Central to this current study is the investigation of crosslinking density of TEAMs on ion-water separation performance and water permeability. Crosslinker proportions were varied by two different strategies that were specifically chosen for PMAA and PMOTA in order to minimize synthesis steps, increase reproducibility, and reduce asymmetry. Although varied %$MI_{Halogen}$ for *x*PMOTA or %*t*BMA for PMAA-*co*-*x*PHEMA theoretically would alter the final crosslinking density, verifying changes in crosslinker density proved challenging. Determination of crosslinking density often requires large, pure samples of polymer for solvent swelling or testing of mechanical properties [82]. These properties of an ultrathin brush polymer layer could not be decoupled from the much thicker support. Binding and eluting probe molecules may work, but this method requires the ability to determine the absolute surface area covered by the brushes and to know the brush molecular weight [12,69]. The absolute surface area of the support membranes, including the walls of tortuous, asymmetric pores, would be at minimum inconsistent between samples if not impossible to measure accurately. Additionally, chemical and physical properties of brush polymers within pores were unlikely to directly match top-surface polymers due to steric and diffusive effects. Thus, measurements of water contact angles, pure water permeability, and ATR-FTIR spectroscopy were employed as clues to successful polymer preparation and crosslinking.

Changes in water contact angles were previously shown to suggest successful modification of cellulose support layers during each synthesis step towards producing BAMs of hydrophilic PHEMA and hydrophobic poly(*tert*-butyl acrylate) (P*t*BA) [69]. Similarly, changes in water contact angles correlated well to precursor, hydrophobic polymers of P*t*BMA and PDMAEMA compared to their corresponding ionizable polymers after modification into PMAA and PMOTA [49]. We hypothesized that the addition of crosslinkers would increase water contact angles because these linkers contain hydrophobic, aliphatic chains. Thus, water contact angles were measured for both *x*PMOTA and PMAA-*co*-*x*PHEMA with varied percentages of $MI_{Halogen}$ and *t*BMA versus crosslinker used during synthesis (Fig. 2a). Indeed, we see an increase in water contact angle with the addition of a crosslinker. The water contact angle of un-crosslinked PMOTA is slightly below that of PMAA, which we attribute to the difference in degree of dissociation of each polymer type. While PMOTA is fully ionized in water, the carboxyl groups in PMAA are only partially deprotonated since it has been reported that PMAA has a pK_a~4–7 and the operating pH was 5.8 ± 0.2 [83–85]. Nevertheless, as crosslinker is added to *x*PMOTA, water contact angle increases at a faster rate per mol% of crosslinker used than for PMAA. That is, when %$MI_{Halogen}$ = 80% for *x*PMOTA, the water contact angle is nearly 90° while when %*t*BMA = 80% for PMAA-*co*-*x*PHEMA, the water contact angle is ~60°. This behavior is not expected since the quaternization of amines by both 1,6-diiodohexane and methyl iodide produces a fully ionizable group whereas esterification of hydroxyl groups with adipoyl chloride produces no ionizable functionalities.

The difference in how both crosslinked membrane types were produced may be responsible for these unexpected trends in water contact angle. For instance, the *x*PMOTA crosslinking reaction involved a competitive bonding process. It is possible that a higher proportion of crosslinker initially bonds to the PMOTA brush polymers at the interface of the active layer and reaction solution. Steric effects as well as differences in diffusivity between methyl iodide and bulkier 1,6-diiodohexane may cause methyl iodide to more readily penetrate and bond faster at greater depths from the surface than crosslinker. Secondly, the two carbonyls present in adipoyl chloride make it less hydrophobic than free 1,6-diiodohexane, as evident in their differing octanol/water partition coefficients (log$P_{oct/wat}$) of 2 and 4.6, respectively [86,87].

A decrease in pure water permeability (PWP) with the addition of crosslinked TEAMs was expected. Previously, we reported the permeability of PMAA, PMOTA, PMAA-*b*-PMOTA, and PMAA-*b*-PMOTA-*b*-PMAA TEAMs with no crosslinking to be in the range of 15–20 L m^{-2} h^{-1} bar^{-1} for DP = 770–1400 for each block [49]. With the addition of a relatively long crosslinker, *x*PMOTA had a reduced PWP = 11 ± 4.5 L m^{-2} h^{-1} bar^{-1} while PMAA-*co*-*x*PHEMA exhibited a PWP = 8.7 ± 1.4 L m^{-2} h^{-1} bar^{-1} (Fig. 2b). Consistently, incorporating shorter crosslinkers at the same proportion as the longer ones reduced PWP even more, with PWP = 5.5 ± 0.6 and 4.5 ± 0.9 L m^{-2} h^{-1} bar^{-1} for *x*PMOTA and PMAA-*co*-*x*PHEMA, respectively. For all concentrations of crosslinkers used when comparing long versus short crosslinkers for *x*PMOTA, average PWP and variance in PWP decreased. (Fig. S3). These results suggest that crosslinker length can affect the pore size, which in turn determines the effective density of charged groups.

ATR-FTIR spectroscopy revealed signature absorbance peaks consistent with these polymer types (Fig. 2c). Key spectral peaks indicating the addition of groups from PMAA and PMOTA include carbonyl stretching at a wavenumber of 1725 cm^{-1}, N^+-CH_3 scissoring at 1560 cm^{-1} for PMOTA, and additional and/or shifted CH_3 and CH_2 peaks. With cellulose taken as the background, the spectral valleys indicate functional groups that are either reduced/removed or shielded from light by the brush active layer, since ATR-FTIR has a limited depth of light penetration. Key valleys for brush-modified membranes include those corresponding to OH stretch at 3300 cm^{-1} and the C–O–C stretch at 1015 cm^{-1}. There was no detectible difference between spectra of the same polyelectrolyte type with varied crosslinker density.

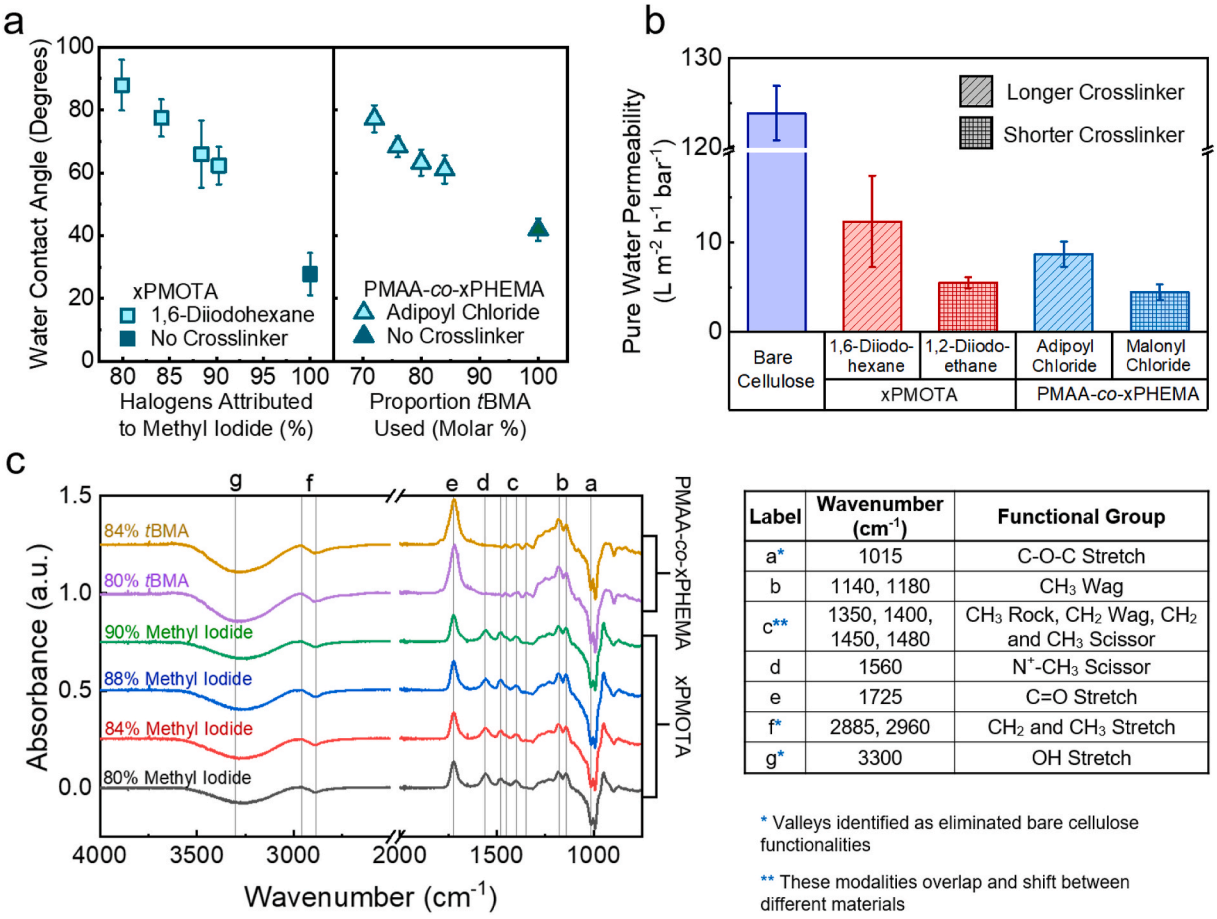

Label	Wavenumber (cm^{-1})	Functional Group
a*	1015	C-O-C Stretch
b	1140, 1180	CH_3 Wag
c**	1350, 1400, 1450, 1480	CH_3 Rock, CH_2 Wag, CH_2 and CH_3 Scissor
d	1560	N^+-CH_3 Scissor
e	1725	C=O Stretch
f*	2885, 2960	CH_2 and CH_3 Stretch
g*	3300	OH Stretch

* Valleys identified as eliminated bare cellulose functionalities

** These modalities overlap and shift between different materials

Fig. 2. Verification of brush layers on cellulosic supports through comparison of material and surface properties. (a) Water contact angles for bare and brush-modified cellulose membranes. Droplets of 1 μL of water were dropped on surfaces. Right and left side contact angles were averaged from profile snapshots taken over a total of 10 s at increments of 0.3 s. Effect on water contact angle with varied crosslinker proportion was probed. For PMAA-*co*-*x*PHEMA, adipoyl chloride was used as crosslinker, and for *x*PMOTA, 1,6-diiodohexane was used. (b) Water permeability of bare and modified membranes, taken in a dead-end cell at a stir rate of 350 rpm. All membranes were tested at 2 bar except the bare membrane (0.7 bar). Relatively long and short crosslinkers were used for both negatively- and positively-charged TEAMs. For *x*PMOTA, $\%MI_{Halogen} = 88\%$ and for PMAA-*co*-*x*PHEMA, $\%t\text{BMA} = 80\%$. (c) ATR-FTIR spectra of modified membranes using various crosslinker densities (left) with corresponding functional groups identified (right). The baseline was taken as the bare cellulose membrane. Membranes were exchanged from water to acetone before drying for 24 h under vacuum. Both peaks and valleys are identified, as valleys signify functional groups present in the bare cellulose membrane that are significantly reduced in the modified membranes. For all blocks in brush-modified membranes, DP = 1300 ± 60 and $Đ = 1.31 \pm 0.07$ (for P*t*BMA) based on a homogeneous polymer produced in the same environment. All error bars represent a standard deviation ($n \geq 3$).

3.2. Single-block TEAMs with relatively short crosslinkers demonstrate the highest co-ion rejection

Before crosslinker was considered for single-block TEAMs, we also conjectured that crosslinking could be used to optimize salt rejection of multiblock TEAMs. Previously, we found that adding more blocks of alternating charge reduced salt rejection of TEAMs [49], unlike the addition of polyelectrolyte bilayers in PEMs [45,46]. Specifically, diblocks of PMAA-*b*-PMOTA on 30 kDa MWCO cellulose supports had rejected only 45 ± 11% and 32 ± 8% of $CaCl_2$ and NaCl, respectively. Meanwhile, single-block TEAMs of PMOTA had rejected 70 ± 4% $CaCl_2$ and 60 ± 5% NaCl. In this new study, we hypothesized that partially crosslinking some layers would improve performance of multiblock TEAMs by minimizing the possibility that blocks of opposite charge were shielding each other through brush collapse into a more entropically-favorable state. Crosslinking could theoretically force like-charges to remain neighbored with like-charges. In producing a diblock TEAM on 10 kDa MWCO cellulose supports using 1,6-diiodohexane to crosslink the terminating layer of PMAA-*b*-*x*PMOTA, we saw improvement of cation rejection over uncrosslinked diblock TEAMs. The crosslinked diblock with $\%MI_{Halogen} = 90\%$ rejected 75 ± 6% $CaCl_2$, 53 ± 5% NaCl, and 4 ± 1% Na_2SO_4 (data not shown in a figure). However, the salt rejection of a single block of PMOTA on 10 kDa MWCO supports has essentially the same performance, rejecting 70 ± 7% $CaCl_2$ and 58 ± 6% NaCl (Fig. 3a). Hence, for the remainder of the study, we focused on crosslinking single-block TEAMs.

Even scrapping the strategy of using crosslinking for better block alignment in multiblock TEAMs, we still hypothesized that crosslinking of single-block TEAMs would enhance salt rejection by ensuring full coverage of pores with charged groups and/or inducing size-based exclusion. It would seem, then, that crosslinker length may also be critical in optimizing salt rejection. Short crosslinkers may pull chains closer together but also be more prone to intramolecular bonding due to reactive end proximity, so we crosslinked TEAMs with both relatively short and long crosslinkers to explore these possible effects.

We found that at a specific proportion of crosslinker incorporated during TEAM synthesis, co-ion salt rejections were maximized and surpassed the water-salt permselectivity of uncrosslinked TEAMs (Fig. 3). For *x*PMOTA, shorter and longer crosslinkers proved to maximize divalent co-ion salt rejections at the same proportion of methyl iodide, when $\%MI_{Halogen} = 88\%$. The maximal $CaCl_2$ rejection was 86 ± 4% using 1,6-diiodohexane and 90 ± 1% using 1,2-diiodoethane. Shorter crosslinker, then, effectively did not enhance divalent co-ion rejection over longer crosslinker. Similarly for PMAA-*co*-*x*PHEMA,

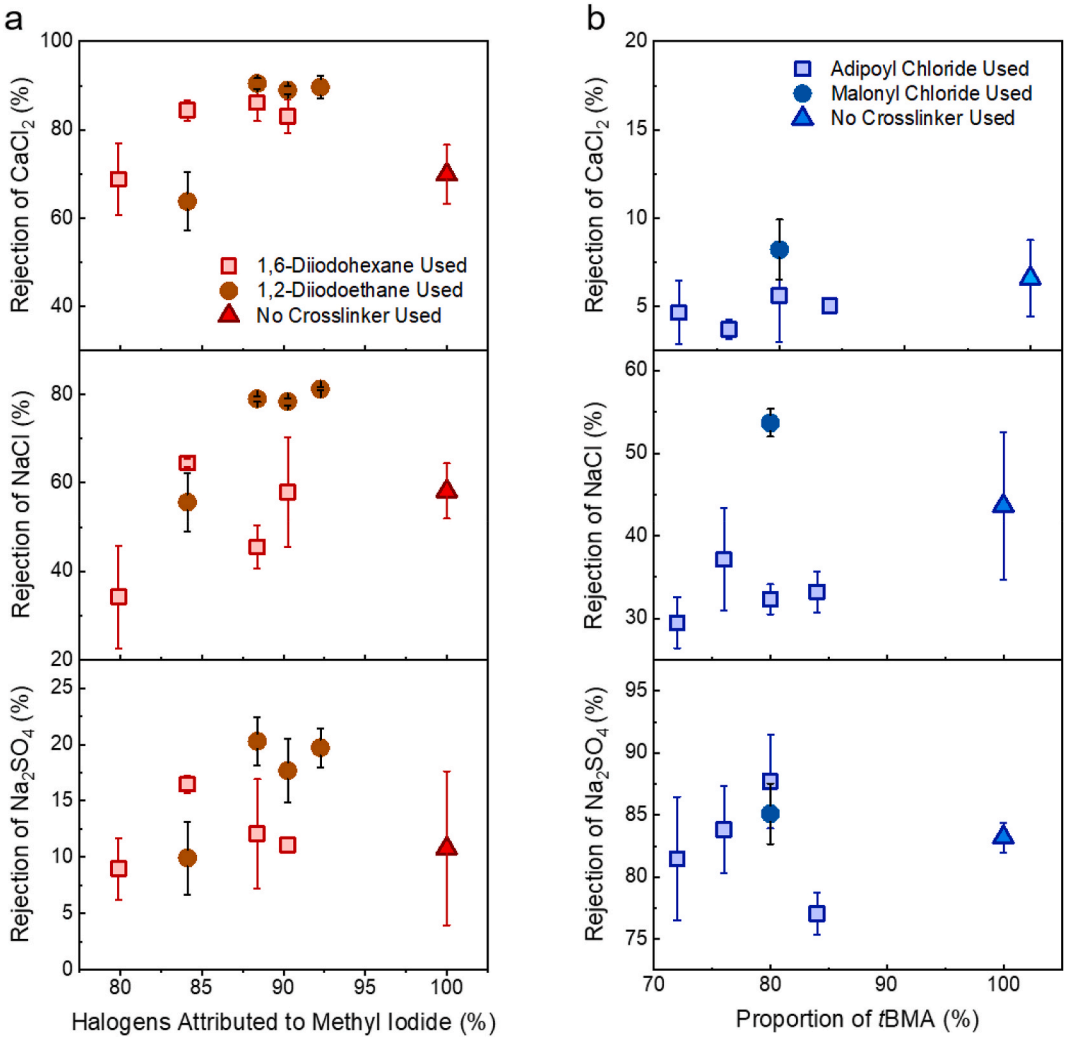

Fig. 3. Salt rejections at varied crosslinker length and proportion. (a) Rejections of $CaCl_2$ (top), NaCl (middle), and Na_2SO_4 (bottom) by *x*PMOTA using various proportions of crosslinkers at both relatively longer (1,6-diiodohexane) and shorter (1,2-diiodoethane) lengths. (b) Rejections of $CaCl_2$ (top), NaCl (middle), and Na_2SO_4 (bottom) by PMAA-*co*-*x*PHEMA using various proportions of crosslinkers at both relatively longer (adipoyl chloride) and shorter (malonyl chloride) lengths. All polymer blocks were DP = 1300 ± 60 and $Đ$ = 1.31 ± 0.07 (for P*t*BMA) based on a homogeneous polymer produced in the same environment. Rejections were conducted in a dead-end cell with a stirring rate of 350 rpm under 2 bar pressure with single-salt concentrations of 2 mM. Error bars represent a standard deviation (n = 3).

rejection of Na_2SO_4 was maximized at a specific proportion of crosslinker adipoyl chloride, when %*t*BMA = 80%. Divalent anion rejection was 88 ± 4%, exceeding the rejection of 83 ± 1% by uncrosslinked PMAA. All *x*PMOTA with varied $\%MI_{Halogen}$ were produced from a single SI-ATRP reaction of PDMAEMA by adjusting subsequent quaternization conditions. Therefore, brush layer qualities were consistent between samples of varied crosslinking proportion. On the other hand, each change in proportion of *t*BMA for PMAA TEAMs required a separate polymerization. Consistently matching molecular weight across all ATRP reactions proved challenging. Therefore, it was assumed that the proportion of crosslinker that would maximize rejection using shorter malonyl chloride would also optimize performance with the longer crosslinker adipoyl chloride, using %*t*BMA = 80% for both crosslinker types. However, rejection of Na_2SO_4 by PMAA-*co*-*x*PHEMA crosslinked using malonyl chloride was 85 ± 2%, which is insignificantly different from rejection by membranes with both longer and no crosslinkers.

Although shorter crosslinkers did not significantly increase rejection of divalent co-ions over TEAMs that incorporated longer crosslinkers, they dramatically increased rejection of monovalent co-ions (Fig. 3). For *x*PMOTA with $\%MI_{Halogen}$ = 88%, NaCl rejection was 45 ± 5 and 79 ± 1% using 1,6-diiodohexane and 1,2-diiodoethane, respectively. For PMAA-*co*-*x*PHEMA with %*t*BMA = 80%, NaCl rejection was 32 ± 2 and 54 ± 2% using adipoyl chloride and malonyl chloride, respectively. Rejection of divalent counterions by all TEAMs was below 20%, although use of shorter crosslinkers did slightly increase these rejections.

We expected that enhanced ion rejection would reduce permeability, following the typical selectivity-permeability tradeoff correlation [47, 48]. Upon reexamining the PWP of TEAMs with optimized crosslinker density (Fig. 2b), we see that with shorter crosslinkers, the permeability was reduced while monovalent ion rejection was enhanced.

Interestingly, precursor polymers exhibited relatively high salt rejection (Fig. S4). PDMAEMA membranes rejected $CaCl_2$, NaCl, and Na_2SO_4 by 93 ± 4, 81 ± 2, and 16 ± 0.5. The unconverted P*t*BMA-*co*-PHEMA with %*t*BMA = 80%, i.e., a membrane comprising primarily hydrophobic pendants with some hydrophilic groups, rejected Na_2SO_4, NaCl, and $CaCl_2$ 96 ± 0.2%, 30 ± 2% and 6 ± 2%, respectively (Fig. S4). However, permeability for these membranes was relatively low, at 0.84 ± 0.1 and 1.73 ± 0.4 L m^{-2} h^{-1} bar^{-1} for PDMAEMA and P*t*BMA-*co*-PHEMA, respectively (Fig. S5). These outcomes suggest BAMs with varied hydrophobic and hydrophilic groups deserve further investigation to understand and optimize selectivity and permeability.

PMAA-*co*-PHEMA with %*t*BMA = 80%, i.e., a negatively charged membrane with a portion of hydroxyl groups and no crosslinking, rejected Na_2SO_4, NaCl, and $CaCl_2$ by 70 ± 19, 32 ± 3, and 1.5 ± 0.5%, respectively. Co-ion rejections were slightly lower than an uncrosslinked PMAA membrane, which is reasonable considering some functional groups are occupied by uncharged PHEMA. This membrane also had a lower permeability than the pure or crosslinked PMAA membranes, at 3.5 ± 1 L m^{-2} h^{-1} bar^{-1} (Fig. S5), likely due to an effective dynamic crosslinking caused by hydrogen bonding between hydroxyl groups. Hydrogen bonding with the permeating water could also increase resistance to permeation. Water contact angles of precursor and uncrosslinked membranes, shown in Fig. S6, are consistent with expectations.

3.3. Ion rejection of crosslinked TEAMs is attributed to primarily charge-based exclusion mechanisms

In order to paint a better picture of transport across crosslinked TEAMs, we considered several clues that differentiate between charge- and size-based exclusion mechanisms. First, upon revisiting salt rejections (Fig. 3), we see that divalent counterions were not highly rejected, even when short crosslinkers were included. If size-exclusion was a key contributor to salt rejection, we would expect significant rejection of larger hydrated divalent ions, regardless of their charge.

Secondly, rejection insights were reinforced through the determination of MWCOs for TEAMs and bare cellulose using various MWs of PEG (Fig. 4a). Note here that the smallest molecule used was raffinose since MWs of PEGs below 1 kDa were not commercially available. We interpolated from these rejections the point at which neutral solutes were rejected 90%, defined as the MWCO. The bare cellulose, which had a MWCO advertised as 10 kDa on the basis of globular protein rejection, exhibited a higher MWCO of ~95 kDa using linear PEGs. After modification with crosslinked TEAMs, MWCO in all cases was reduced. Just as un-crosslinked PMAA previously had a higher MWCO than PMOTA [49], we found that PMAA-*co*-*x*PHEMA had a MWCO higher than *x*PMOTA when relatively long crosslinkers were used. However, using shorter crosslinkers induced MWCOs that were close to 3 kDa for both brush polymer types. This MWCO is larger than typical NF membranes, which highly reject polysaccharides within the range of a few 100 Da with pores of ~1 nm diameter [88,89]. Based on previously developed correlations between effective pore size and PEG-based MWCO [90,91], pore sizes for bare cellulose and PMAA-*co*-*x*PHEMA crosslinked with adipoyl chloride are estimated to be around 14 and 8 nm across, respectively. Meanwhile, we estimate pore diameters for membranes with MWCO ≈3 kDa to be around 3 nm. Although TEAMs with short crosslinkers have smaller pores than ultrafiltration cellulose, they do not come close to the sizes of Cl^-, Na^+, SO_4^{2-} or Ca^{2+} ions in water, which have hydrated diameters of 0.66, 0.72, 0.76, and 0.82 nm, respectively [92]. The size dissimilarity between crosslinked TEAMs and ions involved in rejections further strengthens the argument against size-based exclusion.

While *x*PMOTA membranes produced using shorter crosslinkers exhibited greater salt rejection and lower permeability (Figs. 2 and 3), they did not have a significantly smaller MWCO or pore size (Fig. 4). Water contact angle can help rationalize this behavior (Fig. S6). While *x*PMOTA with $\%MI_{Halogen}$ = 88% produced using 1,6-diiodohexane had a water contact angle of 66 ± 11°, using 1,2-diiodoethane at the same $\%MI_{Halogen}$ resulted in a water contact angle of 98 ± 9°. This can be explained by the method of incorporating crosslinker in these membranes, which promotes asymmetric crosslinking, as described in the previous discussion on water contact angles. A smaller crosslinker with a faster diffusion rate would more competitively bond with methyl iodide at greater depths than a larger crosslinker. However, the shorter crosslinker also has a higher probability of intramolecularly bonding rather than intermolecularly crosslinking, potentially maintaining an average pore size only slightly smaller than with longer crosslinker but a thicker crosslinked layer. While charge may play the greatest role in rejection, hydrophobicity of *x*PMOTA could also hinder water and ion transport.

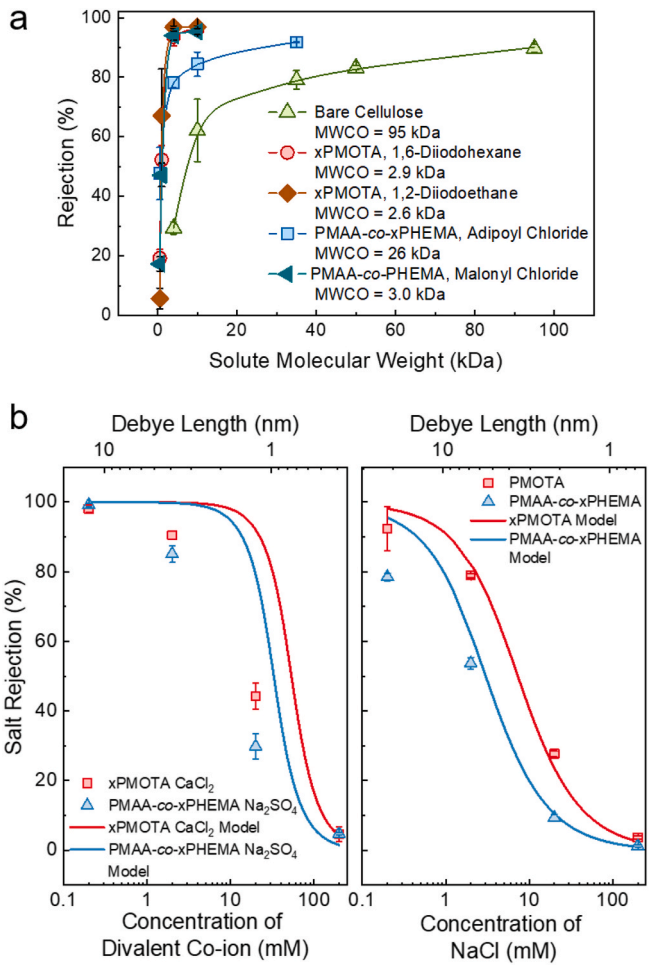

Fig. 4. Evidence that rejection is primarily attributed to charge-based exclusion mechanisms. (a) Molecular weight cutoff (MWCO) for bare and modified membranes with varied crosslinker type. MWCOs were determined using various sizes of PEG, with the exception of the lowest molecular weight at 0.5 kDa being raffinose, all at a concentration of 1000 ppm. (b) Comparison of salt rejections with varied salt concentration and corresponding Debye length for divalent salts (left) and monovalent NaCl ions (right). For *x*PMOTA, $CaCl_2$ was the divalent salt of interest to determine the rejection of calcium, while for PMAA-*co*-*x*PHEMA, Na_2SO_4 was the divalent salt of interest to probe the rejection of the sulfate. Shorter crosslinkers were used for synthesis. The model represented is the Donnan-steric-pore model. In both (a) and (b) for *x*PMOTA, $\%MI_{Halogen}$ = 88% and for PMAA-*co*-*x*PHEMA, %*t*BMA = 80%. Rejection tests were conducted in a dead-end stirred cell at a stirring rate of 350 rpm under 2 bar pressure. The average fluxes for *x*PMOTA and PMAA-*co*-*x*PHEMA in (b) were 13 ± 2 and 8 ± 2 L m^{-2} h^{-1}, respectively. All PMAA polymer blocks were DP = 1300 ± 60 and $Đ$ = 1.31 ± 0.07 (for P*t*BMA) based on homogeneous polymer analogues produced simultaneously in the same environment. Error bars represent a standard deviation (n = 3).

As further proof of the critical role of charge for ion rejection in crosslinked TEAMs, we established how salt rejection changes with Debye length, or the distance at which a charge carrier's electrostatic effect persists and its net electrostatic effect [93]. Increasing ion concentration enhances electrostatic screening, reducing the electric potential of all species and decreasing the Debye length. For a membrane that relies on electrostatic repulsion to reject ions, changing concentration and consequently Debye length should show drastic variation in salt rejection. Therefore, we incrementally varied salt concentration by orders of magnitude, from 0.2 to 200 mM and quantified co-ion rejection of TEAMs produced using short crosslinkers at optimal density (Fig. 4b).

We see that for both *x*PMOTA and PMAA-*co*-*x*PHEMA, NaCl and divalent co-ion rejection were highly dependent on solution concentration, decaying exponentially. We modeled this phenomenon in terms of Donnan exclusion as well, employing the Donnan-steric-pore model (DSPM, details in the *Supplementary Data*). This model ascribes the partitioning mechanisms of salt to the Donnan effects and steric exclusion. After partitioning into the polymer matrix, the ion transport through the membrane is driven by the gradients of electrical potential and ion concentrations in addition to the advective transport [77,94,95].

The model fits the experimental data better for monovalent ions than for divalent ions. Several assumptions and limitations of the model may explain the imperfect fit. First, the model assumes straight cylindrical pores with homogeneous, fixed charge density. However, the flow pathways comprise polymer brushes that are crosslinked at a low crosslinking density. Therefore, the assumed pore diameters based on MWCO likely are not continuous but rather narrower selectivity windows that only persist a fraction of the active-layer thickness. Secondly, the charge density is likely asymmetric, since ionizable groups cannot completely ionize when crowded. It has been shown that at greater depths within ionizable brush polymers at high grafting density, charge density approaches zero [81]. This was accounted for to some degree by assuming a linear degradation in charge density based trends reported in the literature [81], but the overall charge density was still averaged into

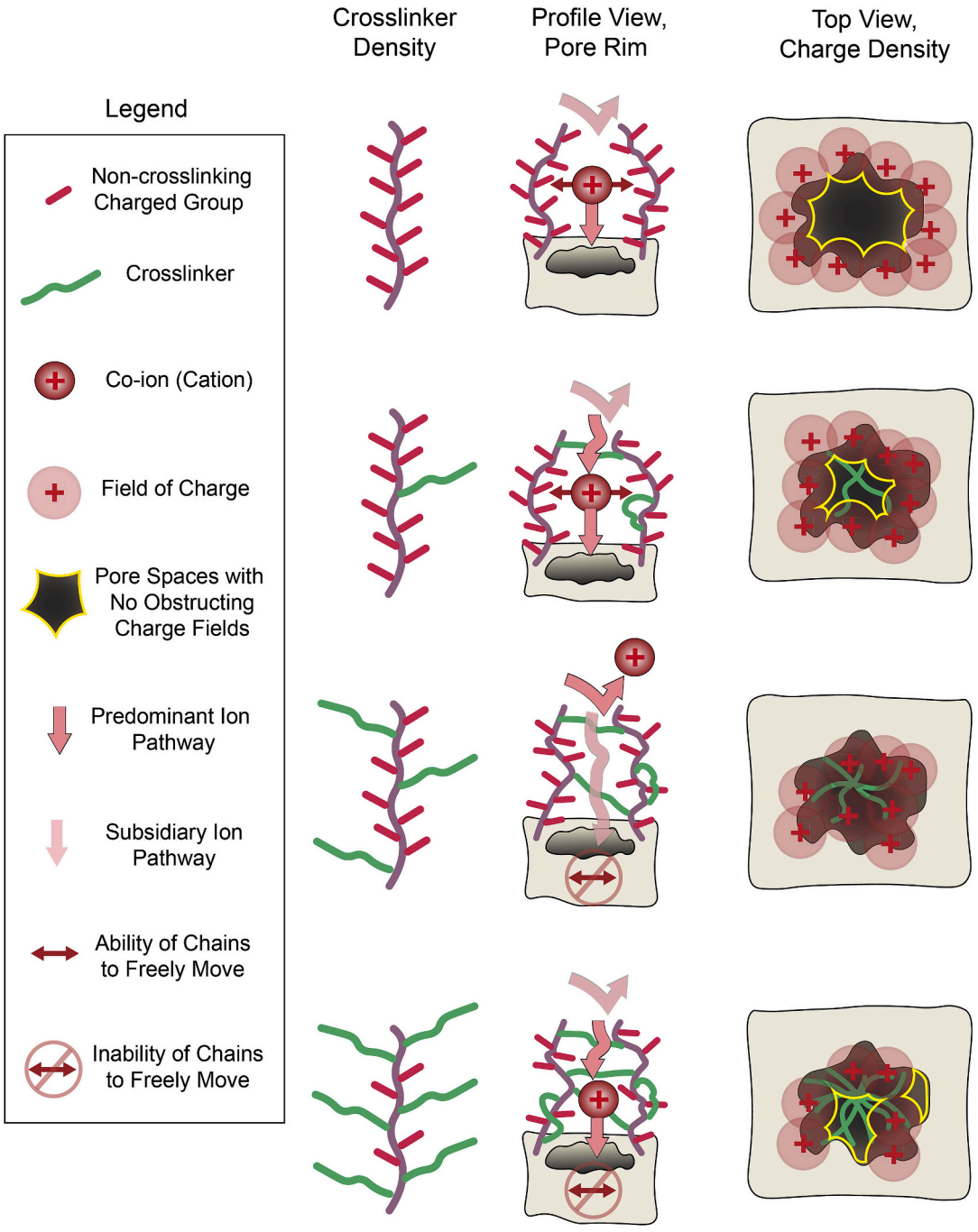

Fig. 5. Proposed mechanisms dictating the importance of a specific crosslinker density in optimizing the effective charge density over pore mouths. *x*PMOTA is depicted, but similar mechanisms are expected for PMAA-*co*-*x*PHEMA. A certain proportion of crosslinker is needed to effectively pull polyelectrolytes grown around pore rims across pores. At relatively higher crosslinker density, aliphatic chains begin to shield charge force fields, reducing the effective Debye length.

a homogeneous distribution. Additionally, the volumetric charge density is estimated based on the areal density of functional groups and the geometry of cylindrical pore. The latter assumption likely neglects the dynamics of the polymer structures and the uncertainty of the pore geometry. Finally, we could not account for how the ions affect the brush conformation and charge density, setting a value that did not change with concentration. The fit suggests charge density was overestimated. Even with these limitations, the general trends of the model

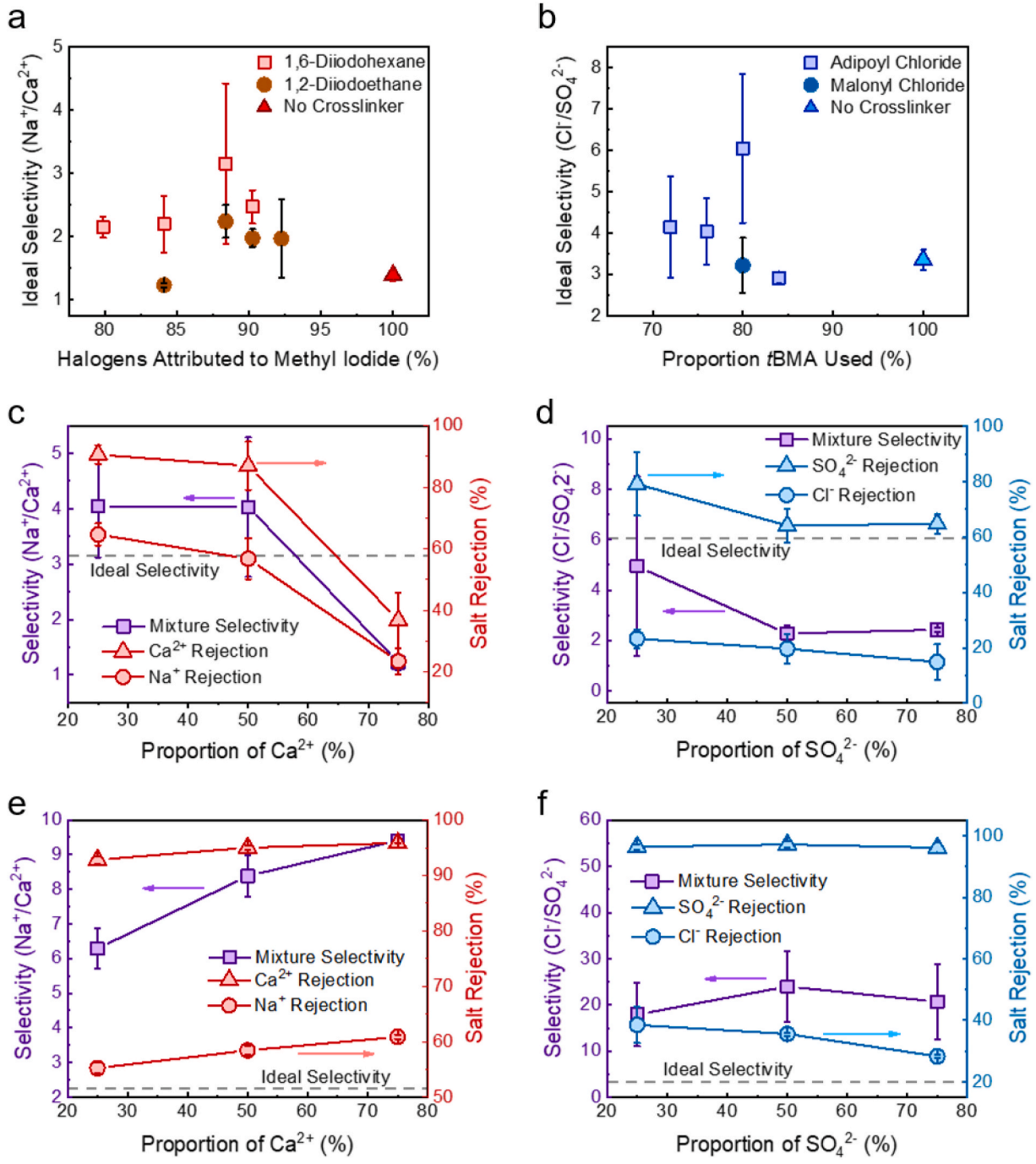

Fig. 6. Monovalent co-ion selectivity for crosslinked tethered electrolyte active-layer membranes (TEAMs). (a) Ideal monovalent selectivity between sodium and calcium ions of *x*PMOTA TEAMs made relatively long and short crosslinkers, 1,6-diiodohexane and 1,2-diiodoethane, respectively. The average fluxes using 1,6-diiodohexane and 1,2-diiodoethane were 18 ± 6 and 11 ± 2 L m^{-2} h^{-1}, respectively. (b) Ideal monovalent selectivity between chloride and sulfate ions of PMAA-*co*-*x*PHEMA TEAMs synthesized using relatively long and short crosslinkers, adipoyl chloride and malonyl chloride, respectively. The average fluxes using adipoyl chloride and malonyl chloride were 17 ± 3 and 9 ± 2 L m^{-2} h^{-1}, respectively. For (a) and (b), ideal selectivity was calculated from single-salt rejection tests at a concentration of 2 mM. (c) Monovalent selectivity of *x*PMOTA TEAMs crosslinked with 1,6-diiodohexane, using mixed salt solutions. (d) Monovalent selectivity of PMAA-*co*-*x*PHEMA TEAMs crosslinked with adipoyl chloride, using mixed salt solutions. (e) Monovalent selectivity of *x*PMOTA TEAMs crosslinked with 1,2-diiodoethane, using mixed salt solutions. (f) Monovalent selectivity of PMAA-*co*-*x*PHEMA TEAMs crosslinked with malonyl chloride, using mixed salt solutions. For (c–f), proportions of monovalent versus divalent co-ions were adjusted, maintaining a total concentration of 2 mM. The DP = 1300 ± 60 and $Đ$ = 1.31 ± 0.07 (for P*t*BMA) based on homogeneous polymer analogues produced simultaneously in the same environment. *x*PMOTA was produced with $\%MI_{Halogen}$ = 88%, and PMAA-*co*-*x*PHEMA was synthesized with %*t*BMA = 80%. Rejection tests were conducted in a dead-end stirred cell at a stirring rate of 350 rpm under 2 bar pressure.

and the observed reduction in salt rejection with increased ion concentration allow us to conclude that crosslinked TEAMs continue to reject primarily by charge-based mechanisms.

We have shown that crosslinkers, especially short ones, can enhance co-ion rejection of TEAMs, with the greatest gains for monovalent solute-water permselectivity. If these linkages are not inducing steric hindrance of ions, then they must be increasing charge effects. The critical area determining transport outcomes of TEAMs is overtop support pores, where brush polymers growing around pore rims are spaced farther apart than across the dense cellulosic surface. For un-crosslinked TEAMs, even if these polymers fan out evenly such that they cover pores in pure water, it is possible that approaching co-ions in electrolyte solutions force these dynamic tethered polymers to shift away from pores, providing more space for ions to bypass charge fields (Fig. 5). The addition of crosslinkers could induce more rigidity, spatially fixing ionized groups atop pores, thereby increasing effective charge density within the primary ion pathways. We envision that the optimal crosslinking density is a balancing act, such that above this quantity, aliphatic chains begin to shield charged groups. Unlike *x*PMOTA whereby all quaternized amines are charged, even when linked to crosslinkers, sidechains used for crosslinking in PMAA-*co*-*x*PHEMA do not produce ionizable groups. Therefore, high crosslinker quantity in PMAA-*co*-*x*PHEMA would reduce effective charge density two-fold, by shielding charge force fields and reducing charge-per-chain. Thus, it makes sense that we saw less enhanced salt rejection by crosslinking PMAA.

3.4. Monovalent selectivity calculated from single-salt rejection underestimates mixed-salt selectivity for TEAMs with shorter crosslinkers

As with any membranes where selectivity is based on electrostatic interactions, there is a limit to the concentration at which ion rejection of TEAMs is significant (Fig. 4). With this limitation, NF and ion-exchange membranes are garnering interest as solute-solute selective platforms for separation of chemically and physically similar charged species [17]. We therefore were interested in proving the monovalent selectivity of crosslinked TEAMs. However, we showed that TEAMs with shorter crosslinkers essentially maintained the same divalent co-ion exclusion as those with longer crosslinkers while enhancing monovalent rejection (Fig. 3). This theoretically would cause reduced monovalent selectivity, as seen with the ideal selectivity calculated from single-salt rejection experiments (Fig. 6a and b). In fact, while ideal selectivity of TEAMs is maximized with longer crosslinkers, TEAMs crosslinked with shorter crosslinkers have ideal selectivity similar or inferior to uncrosslinked TEAMs.

However, in practice with mixed-salt solutions, shorter rather than longer crosslinkers proved to enhance actual mixture selectivity, even at higher proportions of divalent salts (Fig. 6c–f). For these experiments, total co-ion concentration was maintained at 2 mM while proportions of divalent versus monovalent ions were varied between 25, 50, and 75%. With longer crosslinkers, *x*PMOTA exhibited mixture selectivity only slightly higher than ideal with solutions containing cations composed of $\leq$50% Ca^{2+}, and PMAA-*co*-*x*PHEMA fell short of ideal selectivity (Fig. 6c and d). As previously seen with un-crosslinked TEAMs [49], for both these polymer types, an increase in divalent co-ion concentration decreased monovalent selectivity. We attribute this decline to the charge screening caused by a greater concentration of counterions, which reduces both divalent and monovalent rejection. In contrast, as the proportion of $CaCl_2$ increased, *x*PMOTA with shorter crosslinker rejected ions better, resulting in increasing monovalent selectivity (Fig. 6e). At 75% Ca^{2+}, $Na^+/Ca^{2+} = 9.4 \pm 0.1$ and $R_{o,Ca2+} = 96 \pm 0.01\%$. Meanwhile, as the proportion of Na_2SO_4 increased, PMAA-*co*-xPHEMA with shorter crosslinker showed effectively the same selectivity while divalent rejection had no distinct trend and monovalent rejection slightly decreased (Fig. 6f). For these negative membranes, Cl^-/SO_4^{2-} was as high as 24 ± 8% at 50% of each anion type.

If charge shielding by counterions is a key factor, the increase in or maintenance of selectivity with more divalent co-ions for TEAMs with shorter crosslinkers is opposite of anticipated performance. However, this behavior can be explained by the establishment of an electric potential, as smaller counterions can more readily initially cross the oppositely-charged membrane, accelerating the transport of co-ions to maintain electroneutrality [96–98]. When brush polymers are not as rigidly fixed in space, both bulkier monovalent and divalent co-ions can permeate in response to the formation of a membrane potential. However, if pores are smaller and charge density is better maintained, the increase in transport of a smaller species may be disproportionately greater than for the larger, more charged species, as seems the case for PMAA-*co*-*x*PHEMA. As for the *x*PMOTA with shorter crosslinkers, NaCl is rejected far less in mixtures with $CaCl_2$ than in a single-salt solution (i.e., ~50–60% compared to ~80%), which is consistent with the mechanisms of membrane potential. However, as $CaCl_2$ concentration increases, both Ca^{2+} and Na^{2+} are better rejected albeit at a magnitude such that selectivity is still greatly enhanced. That is, from Eq. (5), it is evident that slight changes in divalent rejection have a more drastic effect on monovalent selectivity than changes in monovalent rejection of the same magnitude. Possibly, this counterintuitive increase in selectivity with increasing $CaCl_2$ concentration is still explainable by membrane potential. With more Ca^{2+} than Na^+, reduction in total membrane potential may be caused by the better retention of Ca^{2+} over Na^+. This in turn allows for better retention of all species to maintain electroneutrality.

We attribute the difference in trends between the two types of TEAMs (i.e., positive versus negative) to the effective charge density of each. *x*PMOTA has greater charge per chain than PMAA-*co*-*x*PHEMA because PMOTA amines are fully ionized at neutral pH while PMAA carboxyls are only partially deprotonated. Additionally, the crosslinkers used with *x*PMOTA quaternized amines while crosslinkers in PMAA-*co*-*x*PHEMA produced neutral ester bonds. We also see evidence of this difference in charge density through the response to concentration change (Fig. 4b). When increasing from 0.2 to 2 mM salt concentration, ion rejection by PMAA-*co*-*x*PHEMA decreases at a faster rate than *x*PMOTA. With changes in ion proportions and concentrations, no significant or consistent changes in flux were observed for these crosslinked TEAMs, which is in line with previous results from swelling tests [49].

4. Conclusion

New opportunities for aqueous separations have arisen in recent years, causing a shift away from focus primarily on desalination, towards solute-solute selectivity for resource recovery and treatment of complex, unconventional wastewaters and brines. PEMs, NF, *r*-ZAC-based, and ion-exchange membranes have gained interest as platforms for achieving separations for environmental conservation and sustainable technologies. Strategies have arisen to increase control and tailorability of these membrane types, as biological ion channels suggest specific functional groups at particular spacing are key to increasing selectivity. Natural proteins grow amino-acid-by-amino-acid, suggesting that bottom-up growth of active layers may prove key to mimicking the inspiring performance of nature.

The TEAM, a relatively new form of polyelectrolyte membrane, harnesses this bottom-up concept with controllably and densely grown brush polymers as selective layers. In this study, we have further demonstrated the tailor-ability of TEAMs by adjusting crosslinker ratio and length to enhance salt rejection and monovalent selectivity. Single-block TEAMs crosslinked with relatively short crosslinkers rejected divalent co-ions ~85–95%, and NaCl was rejected ~55 and 80% by negative PMAA-*co*-*x*PHEMA and positive *x*PMOTA, respectively. Cation monovalent selectivity, Na^+/Ca^{2+}, was as high as ~9.5 for *x*PMOTA, while the maximum Cl^-/SO_4^{2-} ratio achieved by PMAA-*co*-*x*PHEMA was ~25. This performance enhancement is attributed to an increase in the effective charge density, as polymers can better cover support layer pores, and functional groups of like-charge are secured closer together.

Even with crosslinking, TEAMs continue to exhibit relatively large MWCOs, which may present opportunities for separations between charged species and neutral solutes, such as specific protein and biomolecular separations.

Even with the improvements demonstrated in this work, TEAMs deserve further investigation to determine if charge density can be further increased, if sized-based exclusion mechanisms can be induced, and if permeance can be enhanced. Regardless, this work reinforces the value of ultrathin brush active-layer membranes and TEAMs as powerful tools to understand fundamental transport of membranes and better control synthesis of polymeric membranes for aqueous separations.

Author statements

Menachem Elimelech: is the adviser of C. Porter, Methodology, Writing - Review & Editing, Supervision, Funding acquisition. **Cassandra Porter**: Conceptualization, Methodology, Formal analysis, Investigation, Writing - Original Draft, Funding acquisition. **Mingjiang Zhong:** is the secondary adviser to C. Porter, Methodology, Writing - Review & Editing, Supervision, Funding acquisition. **Li Wang**: Methodology, Writing - Review & Editing.

Declaration of competing interest

The authors declare that they have no known competing financial interests or personal relationships that could have appeared to influence the work reported in this paper.

Data availability

Data will be made available on request.

Acknowledgements

The transport experimentation work was supported by the U.S. National Science Foundation (NSF) and U.S.-Israel Binational Science Foundation (BSF) under award no. CBET-2110138. The synthesis work was supported by NSF under award no. CHE-1845184. We also acknowledge the NSF Graduate Research Fellowship Program under Grant No. DGE-1752134 and the 2018–2020 NWRI-AMTA Fellowship for Membrane Technology awarded to C.J.P. Any opinions, findings, and conclusions or recommendations expressed in this material are those of the authors and do not necessarily reflect the views of the National Science Foundation, U.S.-Israel Binational Science Foundation, National Water Research Institute, or American Membrane Technology Association. The IC analyzer used for anions was provided by the Yale Analytical and Stable Isotope Center (YASIC). The Yale Chemical and Biophysical Instrumentation Center (CBIC) provided FTIR and NMR equipment.

Appendix A. Supplementary data

Supplementary data to this article can be found online at https://doi.org/10.1016/j.memsci.2022.121214.

References

[1] M. Elimelech, W.A. Phillip, The future of seawater desalination: energy, technology, and the environment, Science 333 (6043) (2011) 712–717.
[2] D.R. Paul, Reformulation of the solution-diffusion theory of reverse osmosis, J. Membr. Sci. 241 (2) (2004) 371–386.
[3] A. Mehta, A.L. Zydney, Permeability and selectivity analysis for ultrafiltration membranes, J. Membr. Sci. 249 (1) (2005) 245–249.
[4] R. Sujanani, et al., Designing solute-tailored selectivity in membranes: perspectives for water reuse and resource recovery, ACS Macro Lett. 9 (11) (2020) 1709–1717.
[5] M.A. Shannon, et al., Science and technology for water purification in the coming decades, Nature 452 (2008) 301.
[6] D.S. Sholl, R.P. Lively, Seven chemical separations to change the world, Nat. News. 532 (7600) (2016) 435.
[7] J.S. Guest, et al., A New Planning and Design Paradigm to Achieve Sustainable Resource Recovery from Wastewater, ACS Publications, 2009.
[8] A. Kumar, et al., Lithium recovery from oil and gas produced water: a need for a growing energy industry, ACS Energy Lett. 4 (6) (2019) 1471–1474.
[9] K. Binnemans, et al., Recovery of rare earths from industrial waste residues: a concise review, in: Proceedings of the 3rd International Slag Valorisation Symposium: the Transition to Sustainable Materials Management, 2013 (Slag Valorisation Symposium).
[10] C. Ayora, et al., Recovery of rare earth elements and yttrium from passive-remediation systems of acid mine drainage, Environ. Sci. Technol. 50 (15) (2016) 8255–8262.
[11] J.R. Werber, A. Desmukh, M. Elimelech, The critical need for increased selectivity, not increased water permeability, for desalination membranes, Environ. Sci. Technol. Lett. 3 (4) (2016) 112–120.
[12] D. Chen, et al., A facile method to quantify the carboxyl group areal density in the active layer of polyamide thin-film composite membranes, J. Membr. Sci. 534 (2017) 100–108.
[13] C.L. Ritt, et al., Ionization behavior of nanoporous polyamide membranes, Proc. Natl. Acad. Sci. USA 117 (48) (2020) 30191–30200.
[14] R. Nagarale, et al., Preparation and electrochemical characterizations of cation-exchange membranes with different functional groups, Colloids Surf. A Physicochem. Eng. Asp. 251 (1–3) (2004) 133–140.
[15] Y. Ji, H. Luo, G.M. Geise, Effects of fixed charge group physicochemistry on anion exchange membrane permselectivity and ion transport, Phys. Chem. Chem. Phys. 22 (14) (2020) 7283–7293.
[16] S.J. Warnock, et al., Engineering Li/Na selectivity in 12-Crown-4–functionalized polymer membranes, Proc. Natl. Acad. Sci. USA 118 (37) (2021).
[17] R.M. DuChanois, et al., Membrane materials for selective ion separations at the water–energy nexus, Adv. Mater. 33 (38) (2021), 2101312.
[18] F. Hua, et al., Fabrication and characterization of metal oxide semiconductor capacitor based on layer-by-layer self-assembled thin films, Nanotechnology 14 (4) (2003) 453–457.
[19] M.L. Bruening, et al., Creation of functional membranes using polyelectrolyte multilayers and polymer brushes, Langmuir 24 (15) (2008) 7663–7673.
[20] P. Bieker, M. Schönhoff, Linear and exponential growth regimes of multilayers of weak polyelectrolytes in dependence on pH, Macromolecules 43 (11) (2010) 5052–5059.
[21] C. Sheng, et al., Facilitated ion transport through polyelectrolyte multilayer films containing metal-binding ligands, J. Membr. Sci. 459 (2014) 169–176.
[22] N. Dizge, et al., Biocatalytic and salt selective multilayer polyelectrolyte nanofiltration membrane, J. Membr. Sci. 549 (2018) 357–365.
[23] L. Li, et al., Effects of acidity on the size of polyaniline-poly(sodium 4-styrenesulfonate) composite particles and the stability of corresponding colloids in water, J. Colloid Interface Sci. 381 (1) (2012) 11–16.
[24] E. te Brinke, et al., Asymmetric polyelectrolyte multilayer membranes with ultrathin separation layers for highly efficient micropollutant removal, Appl. Mater. Today 18 (2020), 100471.
[25] Y. Wang, et al., Removal of emerging wastewater organic contaminants by polyelectrolyte multilayer nanofiltration membranes with tailored selectivity, ACS ES&T Eng. 1 (3) (2021) 404–414.
[26] G. Decher, J.D. Hong, Buildup of ultrathin multilayer films by a self-assembly process: II. Consecutive adsorption of anionic and cationic bipolar amphiphiles and polyelectrolytes on charged surfaces, Ber. Bunsen Ges. Phys. Chem. 95 (11) (1991) 1430–1434.
[27] G. Decher, J. Schmitt, Fine-tuning of the Film Thickness of Ultrathin Multilayer Films Composed of Consecutively Alternating Layers of Anionic and Cationic Polyelectrolytes, Steinkopff, Darmstadt, 1992.
[28] G. Decher, Fuzzy nanoassemblies: toward layered polymeric multicomposites, Science 277 (5330) (1997) 1232–1237.
[29] M. Schönhoff, Layered polyelectrolyte complexes: physics of formation and molecular properties, J. Phys. Condens. Matter 15 (49) (2003) R1781.
[30] N. Joseph, et al., Layer-by-layer preparation of polyelectrolyte multilayer membranes for separation, Polym. Chem. 5 (6) (2014) 1817–1831.
[31] R.M. DuChanois, et al., Designing polymeric membranes with coordination chemistry for high-precision ion separations, Sci. Adv. 8 (9) (2022) eabm9436.
[32] W. Cheng, et al., Selective removal of divalent cations by polyelectrolyte multilayer nanofiltration membrane: role of polyelectrolyte charge, ion size, and ionic strength, J. Membr. Sci. 559 (2018) 98–106.
[33] S.T. Dubas, J.B. Schlenoff, Polyelectrolyte multilayers containing a weak polyacid: construction and deconstruction, Macromolecules 34 (11) (2001) 3736–3740.
[34] M. Ehrmann, J.C. Galin, B. Meurer, Statistical n-butyl acrylate-sulfopropyl betaine copolymers. 3. Domain size determination by solid-state NMR spectroscopy, Macromolecules 26 (5) (1993) 988–993.
[35] T. Wu, et al., Influence of zwitterions on thermomechanical properties and morphology of acrylic copolymers: implications for electroactive applications, Macromolecules 44 (20) (2011) 8056–8063.
[36] P. Bengani, Y. Kou, A. Asatekin, Zwitterionic copolymer self-assembly for fouling resistant, high flux membranes with size-based small molecule selectivity, J. Membr. Sci. 493 (2015) 755–765.
[37] P. Bengani-Lutz, et al., Self-assembling zwitterionic copolymers as membrane selective layers with excellent fouling resistance: effect of zwitterion chemistry, ACS Appl. Mater. Interfaces 9 (24) (2017) 20859–20872.

[38] S.J. Lounder, A. Asatekin, Zwitterionic ion-selective membranes with tunable subnanometer pores and excellent fouling resistance, Chem. Mater. 33 (12) (2021) 4408–4416.
[39] P. Bengani-Lutz, et al., Extremely fouling resistant zwitterionic copolymer membranes with~ 1 nm pore size for treating municipal, oily and textile wastewater streams, J. Membr. Sci. 543 (2017) 184–194.
[40] P. Bengani-Lutz, et al., High flux membranes with ultrathin zwitterionic copolymer selective layers with~ 1 nm pores using an ionic liquid cosolvent, ACS App. Polym. Mater. 1 (8) (2019) 1954–1959.
[41] W. Cheng, et al., Freestanding ultrathin nano-membranes via self-assembly, Nano Today 4 (6) (2009) 482–493.
[42] J. Park, et al., Desalination membranes from pH-controlled and thermally-crosslinked layer-by-layer assembled multilayers, J. Mater. Chem. 20 (11) (2010) 2085–2091.
[43] C. Qiu, S. Qi, C.Y. Tang, Synthesis of high flux forward osmosis membranes by chemically crosslinked layer-by-layer polyelectrolytes, J. Membr. Sci. 381 (1–2) (2011) 74–80.
[44] D. Saeki, et al., Stabilization of layer-by-layer assembled nanofiltration membranes by crosslinking via amide bond formation and siloxane bond formation, J. Membr. Sci. 447 (2013) 128–133.
[45] A. Toutianoush, et al., Polyelectrolyte multilayer membranes for desalination of aqueous salt solutions and seawater under reverse osmosis conditions, Appl. Surf. Sci. 246 (4) (2005) 437–443.
[46] W. Jin, A. Toutianoush, B. Tieke, Use of polyelectrolyte layer-by-layer assemblies as nanofiltration and reverse osmosis membranes, Langmuir 19 (7) (2003) 2550–2553.
[47] L.M. Robeson, The upper bound revisited, J. Membr. Sci. 320 (1) (2008) 390–400.
[48] H.B. Park, et al., Maximizing the right stuff: the trade-off between membrane permeability and selectivity, Science 356 (6343) (2017) eaab0530.
[49] C.J. Porter, et al., Tethered electrolyte active-layer membranes, J. Membr. Sci. 642 (2022), 120004.
[50] B.V. Bhut, S.R. Wickramasinghe, S.M. Husson, Preparation of high-capacity, weak anion-exchange membranes for protein separations using surface-initiated atom transfer radical polymerization, J. Membr. Sci. 325 (1) (2008) 176–183.
[51] S. Zeng, et al., Modification of electrospun regenerate cellulose nanofiber membrane via atom transfer radical polymerization (ATRP) approach as advanced carrier for laccase immobilization, Polymers 13 (2) (2021) 182.
[52] H.H. Himstedt, et al., Responsive membranes for hydrophobic interaction chromatography, J. Membr. Sci. 447 (2013) 335–344.
[53] N. Singh, et al., Modification of regenerated cellulose ultrafiltration membranes by surface-initiated atom transfer radical polymerization, J. Membr. Sci. 311 (1) (2008) 225–234.
[54] E. Ziemann, et al., Zwitterion polymer brushes on porous membranes: characterization, tribology, performance, and the effect of electrolyte anions, ACS App. Polym. Mater. 2 (11) (2020) 4613–4625.
[55] K. Matyjaszewski, J. Xia, Atom transfer radical polymerization, Chem. Rev. 101 (9) (2001) 2921–2990.
[56] K. Matyjaszewski, Atom transfer radical polymerization (ATRP): current status and future perspectives, Macromolecules 45 (10) (2012) 4015–4039.
[57] A. Khabibullin, et al., Surface-initiated atom transfer radical polymerization, in: P. Vana (Ed.), Controlled Radical Polymerization at and from Solid Surfaces, Springer International Publishing, Cham, 2016, pp. 29–76.
[58] D. Zhou, et al., Termination of surface radicals and kinetic modeling of ATRP grafting from flat surfaces by addition of deactivator, Macromolecules 45 (3) (2012) 1198–1207.
[59] T. Erdogan, et al., Well-defined block copolymer ionomers and their blend membranes for proton exchange membrane fuel cell, J. Membr. Sci. 344 (1) (2009) 172–181.
[60] X. Chen, et al., Controlled insulin release from glucose-sensitive self-assembled multilayer films based on 21-arm star polymer, Biomaterials 32 (6) (2011) 1759–1766.
[61] P.-C. Li, et al., Self-assembled structures from PEGylated polypeptide block copolymers synthesized using a combination of ATRP, ROP, and click chemistry, Soft Matter 9 (47) (2013) 11257–11269.
[62] J.I. Clodt, et al., Double stimuli-responsive isoporous membranes via post-modification of pH-sensitive self-assembled diblock copolymer membranes, Adv. Funct. Mater. 23 (6) (2013) 731–738.
[63] J. Ran, et al., Atom transfer radical polymerization (ATRP): a versatile and forceful tool for functional membranes, Prog. Polym. Sci. 39 (1) (2014) 124–144.
[64] A. Venault, et al., Surface self-assembled zwitterionization of poly(vinylidene fluoride) microfiltration membranes via hydrophobic-driven coating for improved blood compatibility, J. Membr. Sci. 454 (2014) 253–263.
[65] A. Alzahrani, et al., Polymerization-induced self-assembly based on ATRP in supercritical carbon dioxide, Polym. Chem. 10 (21) (2019) 2658–2665.
[66] A.W. Mohammad, et al., Nanofiltration membranes review: recent advances and future prospects, Desalination 356 (2015) 226–254.
[67] N. Hilal, et al., Nanofiltration of highly concentrated salt solutions up to seawater salinity, Desalination 184 (1) (2005) 315–326.
[68] S. Hernandez, et al., Layer-by-layer assembled membranes with immobilized porins, RSC Adv. 7 (88) (2017) 56123–56136.
[69] C.J. Porter, et al., Controlled grafting of polymer brush layers from porous cellulosic membranes, J. Membr. Sci. 596 (15) (2020), 117719.
[70] T.W. Greene, P.G. Wuts, Protective Groups in Organic Synthesis, vols. 65–67, John Wiley & Sons Inc, 1999, pp. 404–408.
[71] P. Ye, et al., Synthesis of binary polymer brushes via two-step reverse atom transfer radical polymerization, Macromolecules 44 (7) (2011) 2253–2260.
[72] W. Feng, et al., Surface-initiated atom transfer radical polymerization of oligo (ethylene glycol) methacrylate: effect of solvent on graft density, Macromol. Rapid Commun. 26 (17) (2005) 1383–1388.
[73] R. Chen, et al., Surface-initiated atom transfer radical polymerization grafting of poly(2,2,2-trifluoroethyl methacrylate) from flat silicon wafer surfaces, J. Polym. Sci. Polym. Chem. 44 (3) (2006) 1252–1262.
[74] M.R. Tomlinson, K. Efimenko, J. Genzer, Study of kinetics and macroinitiator efficiency in surface-initiated atom-transfer radical polymerization, Macromolecules 39 (26) (2006) 9049–9056.
[75] J.R. Ell, et al., Structural determination of high density, ATRP grown polystyrene brushes by neutron reflectivity, Macromolecules 42 (24) (2009) 9523–9527.
[76] P.M. Biesheuvel, et al., Tutorial review of reverse osmosis and electrodialysis, J. Membr. Sci. 647 (2022), 120221.
[77] P.M. Biesheuvel, et al., Ion selectivity in brackish water desalination by reverse osmosis: theory, measurements, and implications, Environ. Sci. Technol. Lett. 7 (1) (2020) 42–47.
[78] L. Fetters, et al., Connection between polymer molecular weight, density, chain dimensions, and melt viscoelastic properties, Macromolecules 27 (17) (1994) 4639–4647.
[79] P.C. Hiemenz, T.P. Lodge, Polymer Chemistry, CRC press, 2007.
[80] I. Coluzza, J.-P. Hansen, Transition from highly to fully stretched polymer brushes in good solvent, Phys. Rev. Lett. 100 (1) (2008), 016104.
[81] R. Dong, M. Lindau, C.K. Ober, Dissociation behavior of weak polyelectrolyte brushes on a planar surface, Langmuir 25 (8) (2009) 4774–4779.
[82] C. Hirschl, et al., Determining the degree of crosslinking of ethylene vinyl acetate photovoltaic module encapsulants—a comparative study, Sol. Energy Mater. Sol. Cell. 116 (2013) 203–218.
[83] B. Tian, et al., *Construction of pH-responsive and up-conversion luminescent $NaYF_4$: Yb^{3+}/Er^{3+} @SiO2@PMAA nanocomposite for colon targeted drug delivery*, Sci. Rep. 6 (1) (2016), 21335.
[84] G. Chen, et al., Preparation of pH-sensitive nanoparticles of poly (methacrylic acid) (PMAA)/poly (vinyl pyrrolidone) (PVP) by ATRP-template miniemulsion polymerization in the aqueous solution, Colloid Polym. Sci. 293 (7) (2015) 2035–2044.
[85] B. Dickhaus, R. Priefer, Determination of polyelectrolyte pKa values using surface-to-air tension measurements, Colloids Surf. A Physicochem. Eng. Asp. 488 (2016) 15–19.
[86] PubChem compound summary for CID 61034, adipoyl chloride. National center for biotechnology information:. https://pubchem.ncbi.nlm.nih.gov/compound/Adipoyl-chloride.
[87] PubChem Compound Summary for CID 12373, 1,6-Diiodohexane. National Center for Biotechnology Information.
[88] M.D. Miller, M.L. Bruening, Correlation of the swelling and permeability of polyelectrolyte multilayer films, Chem. Mater. 17 (21) (2005) 5375–5381.
[89] J. Shi, et al., Composite polyelectrolyte multilayer membranes for oligosaccharides nanofiltration separation, Carbohydr. Polym. 94 (1) (2013) 106–113.
[90] S. Lentsch, P. Aimar, J.L. Orozco, Separation albumin–PEG: transmission of PEG through ultrafiltration membranes, Biotechnol. Bioeng. 41 (11) (1993) 1039–1047.
[91] K.J. Howe, M.M. Clark, Fouling of microfiltration and ultrafiltration membranes by natural waters, Environ. Sci. Technol. 36 (16) (2002) 3571–3576.
[92] E. Nightingale Jr., Phenomenological theory of ion solvation. Effective radii of hydrated ions, J. Phys. Chem. 63 (9) (1959) 1381–1387.
[93] P. Debye, E. Hückel, De la theorie des electrolytes. I. abaissement du point de congelation et phenomenes associes, Phys. Z. 24 (9) (1923) 185–206.
[94] O. Labban, et al., Fundamentals of low-pressure nanofiltration: membrane characterization, modeling, and understanding the multi-ionic interactions in water softening, J. Membr. Sci. 521 (2017) 18–32.
[95] L. Wang, et al., Salt and water transport in reverse osmosis membranes: beyond the solution-diffusion model, Environ. Sci. Technol. 55 (24) (2021) 16665–16675.
[96] S.H. Wright, Generation of resting membrane potential, Adv. Physiol. Educ. 28 (4) (2004) 139–142.
[97] A. Galama, et al., On the origin of the membrane potential arising across densely charged ion exchange membranes: how well does the Teorell-Meyer-Sievers theory work? J. Membr. Sci. Res. 2 (3) (2016) 128–140.
[98] X. Zhou, et al., Intrapore energy barriers govern ion transport and selectivity of desalination membranes, Sci. Adv. 6 (48) (2020) eabd9045.